International Journal of Damage Mechanics
http://ijd.sagepub.com/

Numerical Modeling of Fatigue Crack Growth in Single Crystals Based on Microdamage Theory

Ozgur Aslan, Stéphane Quilici and Samuel Forest

International Journal of Damage Mechanics published online 28 January 2011
DOI: 10.1177/1056789510395738

The online version of this article can be found at:
http://ijd.sagepub.com/content/early/2011/01/22/1056789510395738

Published by:
SAGE
http://www.sagepublications.com

Numerical Modeling of Fatigue Crack Growth in Single Crystals Based on Microdamage Theory

Ozgur Aslan,* Stéphane Quilici and Samuel Forest
Centre des Matériaux, Mines ParisTech, UMR CNRS 7633, BP87, 91003 Evry Cedex, France

ABSTRACT: Proper life-time prediction modeling of single crystalline components is of increasing importance due to their common use in turbine industry. Viscoplastic damage approaches are of great interest in that context. However, mechanical properties of single crystals are strongly anisotropic and nonlinear in service conditions, bringing certain complexity into constitutive and numerical modeling. The aim of this work is to develop a thermodynamically consistent constitutive model based on generalized continua in order to simulate fatigue crack initiation and growth in single crystals. For that purpose, a standard crystal plasticity model is taken as a basis and coupled with the continuous damage model developed by Marchal et al. (2006a) [Marchal, N., Forest, S., Remy, L. and Duvinage, S. (2006a). Simulation of Fatigue Crack Growth in Single Crystal Superalloys Using Local Approach to Fracture, In: Moinereau, D., Steglich, D. and Besson, J. (eds.), *Local Approach to Fracture, 9th European Mechanics of Materials Conference, Euromech–Mechamat*, Moret–Sur–Loing, France, Presses de l'Ecole des mines de Paris, pp. 353–358]. As a variant of micromorphic theory, microdamage approach is applied to the model in order to obtain a regularized continuum damage formulation which solves mesh dependency problem by introducing an intrinsic length scale. A detailed finite element implementation procedure and its validation for monotonic crack growth are-shown. Fatigue crack growth analyses have been performed on a single edge notched geometry and a comparison between numerical and experimental results is presented.

KEY WORDS: crystal plasticity, damage mechanics, ductile fracture, localization, crack growth, regularization, micromorphic theory.

*Author to whom correspondence should be addressed. Email: ozgur.aslan@ensmp.fr
Figures 2–4, 6–11 and 13–15 appear in color online: http://ijd.sagepub.com

1056-7895/11/00 0001–26 $10.00/0 DOI: 10.1177/1056789510395738

INTRODUCTION

THE PROPER MODELING of crack growth under cyclic loading is essential for the life-time assessment of single crystals. A deep understanding of plasticity and fatigue damage is necessary for a realistic coupling of these two phenomena resulting in crack initiation and propagation. For instance, a node release technique (Kiyak et al., 2007) is uncoupled and does not consider crack initiation under fatigue loading, although the plastic zones are well described and crack openings are well predicted. In that sense, this approach cannot be considered as fully predictive.

In the literature, there have been many attempts which consider a coupling between plasticity and damage generally formalized in the framework of continuum damage mechanics. The models present a weak coupling (Simo and Ju, 1989; Lemaitre and Chaboche, 1994; Murakami et al., 1998) possess two independent flow rules for damage and plasticity which is not realistic for life-time prediction modeling under fatigue loading. Moreover, there are other attempts proposing a relatively strong coupling considering a single associated flow rule for the evolutions of plasticity and damage (Gurson, 1977; Tvergaard and Needleman, 1984; Mahnken, 2002). Another possible way of coupling could be keeping the flow rules separate but strongly relating the potentials for plasticity and damage, i.e., each flow rule becomes strongly dependent on the other as proposed in (Voyiadjis and Deliktas, 2000; Musienko and Cailletaud, 2009).

Concerning crystallographic materials, strong relation between plasticity and crack growth has been shown by (Leverant and Gell, 1975; Crompton and Martin, 1984; Aswath, 1994). The first attempt to use a plasticity theory to model crack growth has been performed by (Rice, 1987). The crack tip plastic zones in a single crystal grain were further studied by (Gall et al., 1996). In connection with the latter approach (Voyiadjis and Deliktas, 2000), damage localization has been associated to the crystallographic planes and inelastic deformations (Qi and Bertram, 1999; Ekh et al., 2004). A recent predictive cohesive approach has also been proposed by (Bouvard et al., 2009), where plasticity and damage are coupled in order to model creep-fatigue crack growth in single crystals with a prescribed crack path.

The model presented in this article associates damage to each $\{1\,1\,1\}$ plane in FCC crystals where the damage initiation is strongly related with accumulated plastic slip as it was formerly proposed by Marchal et al. (2006a). For every damage plane, three damage systems are defined. The first system represents an opening system, while the other two stand for in-plane deformations in order to simulate mode II and mode III loadings and to enable arbitrary displacements after fracture. The main advantage of the approach

against the methods with prescribed crack paths, like cohesive zone model (CZM) (Bouvard et al., 2009), is the multi-plane damage descriptions which allow to simulate nonstraight crack paths with branching and crack bifurcation.

In the previous work (Aslan and Forest, 2009), mesh dependency of the model for brittle damage has been overcome by a regularization procedure based on microdamage theory derived from micromorphic approach introduced by (Eringen and Suhubi, 1964). The main motivation for switching to a higher order continuum theory was introducing an intrinsic length-scale in order to capture size effects and to deal with mesh size and alignment dependency of the approach within a thermodynamically consistent framework. The main objective of this article is to propose a continuum damage crystal plasticity strategy in order to simulate crack growth in a single crystal under fatigue loading. In particular, a regularization procedure is proposed to ensure mesh independence of the finite element simulation results. For that purpose, first of all, an updated formulation of the coupled approach is given. Secondly, the theory is shown to be well suited for a finite element formulation and a detailed implementation procedure of an implicit scheme is presented. Afterwards, the numerical model is validated for monotonic loading. Finally, finite element analysis of a single edge notched (SEN) specimen is demonstrated and a comparison between numerical and experimental results has been done.

STRAIN-BASED DAMAGE MODEL COUPLED WITH CRYSTAL PLASTICITY

In this model, viscoplasticity and damage are coupled by introducing an additional damage strain variable $\dot{\underset{\sim}{\varepsilon}}^d$, into the strain rate partition equation:

$$\dot{\underset{\sim}{\varepsilon}} = \dot{\underset{\sim}{\varepsilon}}^e + \dot{\underset{\sim}{\varepsilon}}^p + \dot{\underset{\sim}{\varepsilon}}^d \tag{1}$$

where $\dot{\underset{\sim}{\varepsilon}}^e$ and $\dot{\underset{\sim}{\varepsilon}}^p$ are the elastic and the plastic strain rates, respectively. The elastic response of the model takes the standard form:

$$\underset{\sim}{\boldsymbol{\sigma}} = \underset{\approx}{\boldsymbol{c}} : \underset{\sim}{\boldsymbol{\varepsilon}}^e \tag{2}$$

In principle, the elastic properties should be affected by damage. However, following the tradition in ductile fracture Besson (2009), it may be neglected when the damage strain is significantly higher than elastic strain. Therefore, the damage is defined as a strain-like variable and material softening is achieved through the damage criteria defined in Equations (9) and (10).

The flow rule for plastic part is written at the slip system level and the plastic strain rate $\dot{\underset{\sim}{\varepsilon}}^p$ is obtained with the orientation tensor $\underset{\sim}{\boldsymbol{m}}^s$:

$$\underset{\sim}{\boldsymbol{m}}^s = \frac{1}{2}(\underline{\boldsymbol{n}}^s \otimes \underline{\boldsymbol{l}}^s + \underline{\boldsymbol{l}}^s \otimes \underline{\boldsymbol{n}}^s) \tag{3}$$

where $\underline{\boldsymbol{n}}^s$ is the normal to the plane of slip system s and $\underline{\boldsymbol{l}}^s$ stands for the corresponding slip direction. Then, plastic strain rate reads:

$$\dot{\underset{\sim}{\varepsilon}}^p = \sum_{s=1}^{N_{\text{slip}}} \dot{\gamma}^s \underline{\boldsymbol{m}}^s \tag{4}$$

The flow rule on slip system s is a classical Norton rule with threshold.

$$\dot{\gamma}^s = \left\langle \frac{|\tau^s - x^s| - r^s}{K} \right\rangle^n \text{sign}(\tau^s - x^s) \tag{5}$$

where r^s and x^s are the variables for isotropic and kinematic hardening, respectively and K and n are the material parameters to be fit (Nouailhas and Cailletaud, 1995). In this study, isotropic hardening is considered constant and no interaction between slip systems is accounted. Therefore, isotropic hardening becomes:

$$r^s = r_0 \tag{6}$$

The kinematic hardening is taken as nonlinear:

$$x^s = C\alpha^s \quad \text{with} \quad \dot{\alpha}^s = \dot{\gamma}^s - D\dot{\nu}^s\alpha^s \tag{7}$$

where C and D are material constants and $\dot{\nu}^s = |\dot{\gamma}^s|$.

The damage strain $\dot{\underset{\sim}{\varepsilon}}^d$ is decomposed in the following crystallographic contributions:

$$\dot{\underset{\sim}{\varepsilon}}^d = \sum_{s=1}^{N_{\text{damage}}} \dot{\delta}_c^s \underline{\boldsymbol{n}}_d^s \otimes \underline{\boldsymbol{n}}_d^s + \dot{\delta}_1^s \underline{\boldsymbol{n}}_d^s \overset{\text{sym}}{\otimes} \underline{\boldsymbol{l}}_{d_1}^s + \dot{\delta}_2^s \underline{\boldsymbol{n}}_d^s \overset{\text{sym}}{\otimes} \underline{\boldsymbol{l}}_{d_2}^s \tag{8}$$

where $\dot{\delta}^s$, $\dot{\delta}_1^s$ and $\dot{\delta}_2^s$ are the strain rates for mode I, mode II, and mode III crack growth, respectively and N_{damage}^d stands for the number of damage planes which are fixed crystallographic planes depending on the crystal structure. Cleavage damage is represented by the opening δ^s of crystallographic cleavage planes with the normal vector $\underline{\boldsymbol{n}}^s$ and other damage systems must be introduced for the in-plane accommodation along orthogonal directions $\underline{\boldsymbol{l}}_1^s$ and $\underline{\boldsymbol{l}}_2^s$, once cleavage has started (Figure 1). Material separation is assumed to take place with respect to specific crystallographic planes, $\{1\,1\,1\}$. In this study, even though the term cleavage refers to the crack

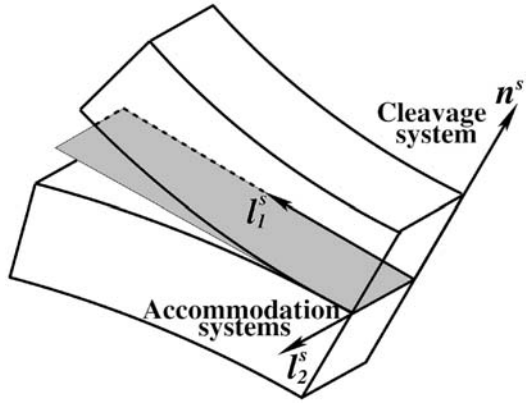

Figure 1. *Illustration of the cleavage and two accommodation systems to be associated to the crystallographic planes.*

opening defined for mode I; it actually does not imply a physical metal cleavage phenomenon which is not directly observed in single crystal nickel base superalloys.

Three damage criteria are associated to one cleavage and two accommodation systems:

$$f_c^s = \left| \underline{\boldsymbol{n}}_d^s \cdot \underset{\sim}{\boldsymbol{\sigma}} \cdot \underline{\boldsymbol{n}}_d^s \right| - Y_c^s \tag{9}$$

$$f_i^s = \left| \underline{\boldsymbol{n}}_d^s \cdot \underset{\sim}{\boldsymbol{\sigma}} \cdot \underline{\boldsymbol{l}}_{d_i}^s \right| - Y_i^s \quad (i = 1, 2) \tag{10}$$

The critical normal stress Y^s for damage decreases as δ increases:

$$Y_c^s = Y_0^s + H\delta_c^s \,, \quad Y_i^s = Y_0^s + H\delta_i^s \tag{11}$$

where Y_0^s is the initial damage stress (usually coupled to plasticity) and H is a negative modulus which controls material softening due to damage. Finally, evolution of damage is given by the following equations;

$$\dot{\delta}_c^s = \left\langle \frac{f_c^s}{K_d} \right\rangle^{n_d} \operatorname{sign}\left(\underline{\boldsymbol{n}}_d^s \cdot \underset{\sim}{\boldsymbol{\sigma}} \cdot \underline{\boldsymbol{n}}_d^s \right) \tag{12}$$

$$\dot{\delta}_i^s = \left\langle \frac{f_i^s}{K_d} \right\rangle^{n_d} \operatorname{sign}\left(\underline{\boldsymbol{n}}_d^s \cdot \underset{\sim}{\boldsymbol{\sigma}} \cdot \underline{\boldsymbol{l}}_{d_i}^s \right) \tag{13}$$

where K_d and n_d are material parameters.

These equations hold for all conditions except when the crack is closed ($\delta_c^s < 0$) and compressive forces are applied ($\underline{\boldsymbol{n}}_d^s \cdot \tilde{\boldsymbol{\sigma}} \cdot \underline{\boldsymbol{n}}_d^s < 0$). In this case, damage evolution stops ($\dot{\delta}_c^s = \dot{\delta}_i^s = 0$), due to the unilateral damage conditions (a detailed explanation is provided in the next section).

Coupling between plasticity and damage is generated through initial damage stress Y_0 in (11) which is controlled by cumulative slip variable γ_{cum}:

$$\dot{\gamma}_{\text{cum}} = \sum_{s=1}^{N_{\text{slips}}} |\dot{\gamma}^s| \tag{14}$$

Then, Y_0 takes the form:

$$Y_0^s = \sigma_n^c \, e^{-\Theta \gamma_{\text{cum}}} + \sigma_{\text{ult}} \tag{15}$$

This formulation suggests an exponential decaying regime from a preferably high initial cleavage stress value σ_n^c, to an ultimate stress, σ_{ult} which is close to but not equal to zero for numerical reasons and Θ is the parameter controlling the coupling rate. Note that the coupling established in this approach is not reciprocal. The coupling between plane separation and plasticity is justified by the following physical metallurgical fact. When dislocations accumulate at some location in a crystal, local stresses become higher and can trigger plane separation, or even cleavage like in zinc (Parisot et al., 2004). The reverse coupling of damage on plasticity has no clear physical interpretation simply because the damage mechanisms are in fact intrinsically linked to plasticity. Therefore, the coupling is performed only in one way.

This model, complemented by the suitable constitutive equations for viscoplastic strain, has been used for the simulation of crack growth under complex cyclic loading at high temperature (Marchal et al., 2006b). Significant mesh dependency of results was found (Marchal, 2006). In this study, regularization of damage field is achieved by switching from classical to microdamage continuum as proposed in (Aslan and Forest, 2009).

MICRODAMAGE CONTINUUM

The foundation of the microdamage continuum lies in micromorphic theory introduced by (Eringen and Suhubi, 1964) which introduces a full microdeformation field χ, in addition to the classical displacement field $\underline{\boldsymbol{u}}$. Containing additional degrees of freedom and balance equations, the micromorphic continuum approach can be considered as the main framework for most generalized continuum models Forest (2009).

Alternative micromorphic variables other than the full strain tensor can be chosen Forest (2009). The strain gradient effect can be introduced through the gradient of damage strain, $\underset{\sim}{\varepsilon}^d$ and more specifically through the gradient of cumulative damage variable, δ_{cum}.

$$\dot{\delta}_{\text{cum}} = \sum_{s=1}^{N_{\text{planes}}} |\dot{\delta}_c^s| + |\dot{\delta}_1^s| + |\dot{\delta}_2^s| \tag{16}$$

Balance and Constitutive Equations

In microdamage theory, the selected microvariable is a scalar microdamage degree of freedom (DOF) ${}^{\chi}\delta$, in addition to the displacement DOFs $\underline{\boldsymbol{u}}$. The DOFs and the extended state space on which constitutive functions may depend are as follows:

$$\text{DOF} = \{\underline{\boldsymbol{u}},\ {}^{\chi}\delta\} \qquad \text{STRAIN} = \{\underset{\sim}{\varepsilon},\ {}^{\chi}\delta, \nabla\, {}^{\chi}\delta\} \tag{17}$$

The power of internal forces is extended as

$$p^{(i)} = \underset{\sim}{\boldsymbol{\sigma}} : \dot{\underset{\sim}{\varepsilon}} + a\, {}^{\chi}\dot{\delta} + \underline{\boldsymbol{b}}.\nabla\, {}^{\chi}\dot{\delta} \tag{18}$$

where generalized stresses a, $\underline{\boldsymbol{b}}$ have been introduced. The generalized balance equations are (Aslan and Forest, 2009):

$$\text{div}\ \underset{\sim}{\boldsymbol{\sigma}} = 0, \tag{19}$$

$$a = \text{div}\ \underline{\boldsymbol{b}} \tag{20}$$

The boundary conditions for the traction vector $\underline{\boldsymbol{t}}$ and generalized traction a_c reads:

$$\underline{\boldsymbol{t}} = \underset{\sim}{\boldsymbol{\sigma}}.\underline{\boldsymbol{n}}, \quad a_c = \underline{\boldsymbol{b}}.\underline{\boldsymbol{n}} \tag{21}$$

The free energy density is taken as a quadratic potential in the elastic strain, damage δ, relative damage $\delta_{\text{cum}} - {}^{\chi}\delta$ and microdamage gradient $\nabla^{\chi}\delta$:

$$\rho\psi = \frac{1}{2}\underset{\sim}{\varepsilon}^e : \underset{\approx}{\boldsymbol{c}} : \underset{\sim}{\varepsilon}^e + \frac{1}{2}\sum_{s=1}^{N_{\text{damage}}} H\delta_s^2 + \frac{1}{2}\,{}^{\chi}H(\delta_{\text{cum}} - {}^{\chi}\delta)^2 + \frac{1}{2}A\nabla^{\chi}\delta\nabla^{\chi}\delta \tag{22}$$

where H, ${}^{\chi}H$ and A are scalar material constants. Then, the elastic response of the material becomes:

$$\underset{\sim}{\boldsymbol{\sigma}} = \rho\frac{\partial\psi}{\partial\underset{\sim}{\boldsymbol{\varepsilon}}^e} = \underset{\approx}{\boldsymbol{c}} : \underset{\sim}{\varepsilon}^e \tag{23}$$

The generalized stresses read:

$$a = \rho \frac{\partial \psi}{\partial {}^{\chi}\delta} = -\,{}^{\chi}H(\delta_{\text{cum}} - {}^{\chi}\delta)\ , \qquad \underline{\boldsymbol{b}} = A\nabla {}^{\chi}\delta \tag{24}$$

and the driving force for each damage system can be derived as:

$$Y^s = \rho \frac{\partial \psi}{\partial \delta^s} = H\delta^s + {}^{\chi}H(\delta_{\text{cum}} - {}^{\chi}\delta) \tag{25}$$

The damage criterion now is:

$$f^s = \left| \underline{\boldsymbol{n}}^s \cdot \underset{\sim}{\boldsymbol{\sigma}} \cdot \underline{\boldsymbol{n}}^s \right| - Y_c = 0 \tag{26}$$

where Y_c is the critical stress for the damage evolution.

$$Y_c = Y_0 + Y^s \tag{27}$$

Inserting the generalized stress terms into the balance law (20) and assuming homogeneous material properties, the following differential form can be deduced:

$${}^{\chi}\delta - \frac{A}{{}^{\chi}H}\Delta {}^{\chi}\delta = \delta_{\text{cum}} \tag{28}$$

where the macrodamage δ_{cum} can be considered as a source term. As previously mentioned in (Aslan and Forest, 2009), this type of Helmholtz equations appear in the so–called implicit gradient theory and it is variants, as an additional equilibrium equation (Peerlings et al., 2001, 2004; Engelen et al., 2003; Germain et al., 2007). However, in these approaches generalized stresses a and $\underline{\boldsymbol{b}}$ are not explicitly introduced and the microvariables are called non-local variables (Dillard et al., 2006; Forest, 2009). Note that the relative damage term, $(\delta_{\text{cum}} - {}^{\chi}\delta)$ is introduced in the free energy density function, $\rho\psi$. A very high value of ${}^{\chi}H$ results in an excessive contribution to the free energy which appears as a penalization term. Therefore, considering an admissible solution of a mechanics problem, a high value of ${}^{\chi}H$ keeps the relative damage term minimum like in a Lagrangian optimization problem and the value of δ_{cum} is enforced to be close to ${}^{\chi}\delta$. In the limit case, $(\delta_{\text{cum}} = {}^{\chi}\delta)$, the formulation leads to a gradient model.

Analysis of 1D Bar

In order to demonstrate the regularization capabilities of the approach and investigate the crack closure phenomenon under fatigue loading, a bar with a length of 2.5 mm under tension is studied (Figure 2). A cleavage plane

normal to direction 2 is taken and an initial defect is introduced at the center with a slightly reduced initial damage threshold.

Recalling the work (Aslan and Forest, 2009), it is known that for pure damage case the solution for ${}^{\chi}\delta$ is sinusoidal

$$ {}^{\chi}\delta = \alpha \sin(\omega x_2) + \beta \cos(\omega x_2) + \gamma \tag{29} $$

where $\omega = \sqrt{|H\ {}^{\chi}H/A(H + {}^{\chi}H)|}$ and the solutions for ε_{22} and δ are of the same type with different constants. Figure 3 demonstrates the harmonic solutions for ${}^{\chi}\delta$ and δ. It is worth mentioning that the penalization between microdamage and damage variable in the damage criterion (22), ${}^{\chi}H(\delta_{\text{cum}} - {}^{\chi}\delta)$, stabilizes the softening term, $H\delta$; therefore, the critical

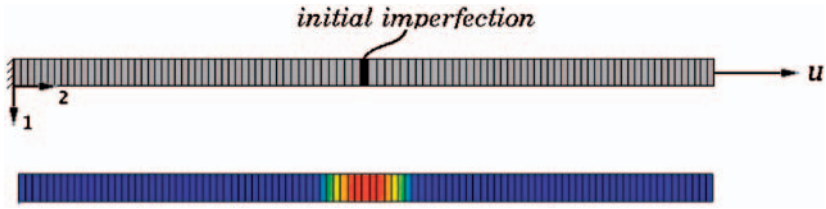

Figure 2. *1D rod under tension with an initial imperfection and the regularization of damage field after a finite element analysis. Field variable δ_{cum} (A=500 MPa.mm^2, H=−15,000 MPa, ${}^{\chi}H$=30,000 MPa, σ_c^n=1000 MPa, σ_{ult}=1000 MPa).*

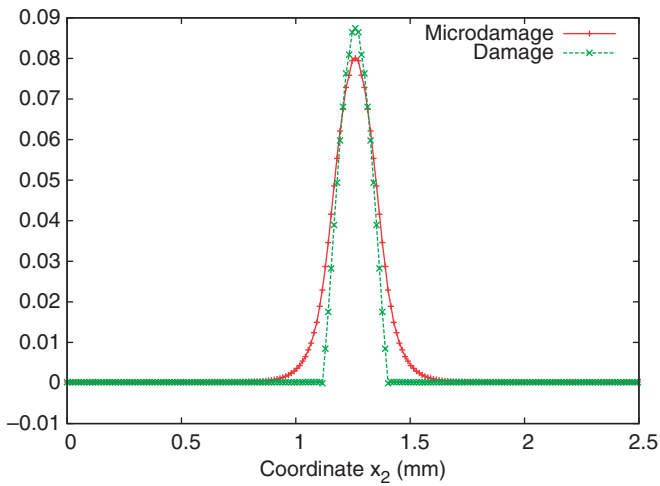

Figure 3. *Comparison of damage and microdamage values penalized in free energy density function (22).*

stress for damage evolution takes the same value throughout the regularized damage zone (Figure 4).

when a material element is broken, the stored energy, especially the energy stored by generalized stresses should vanish. Therefore, an exponential drop for the modulus A is suggested:

$$\underline{\boldsymbol{b}} = Ae^{-Q\delta_{\text{cum}}} \nabla \, {}^{\chi}\delta \tag{30}$$

where Q is a material parameter. Note that due to the decay of the modulus A, the characteristic length starts to shrink which results in a steeper softening regime as it is illustrated in Figure 5.

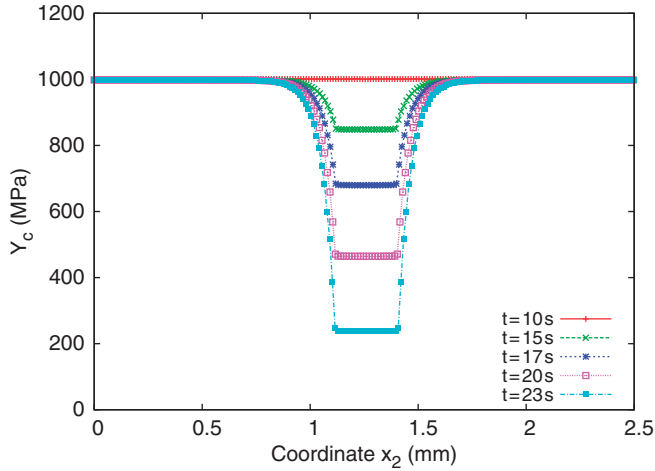

Figure 4. *Evolution of critical damage stress stabilized throughout the damaged zone.*

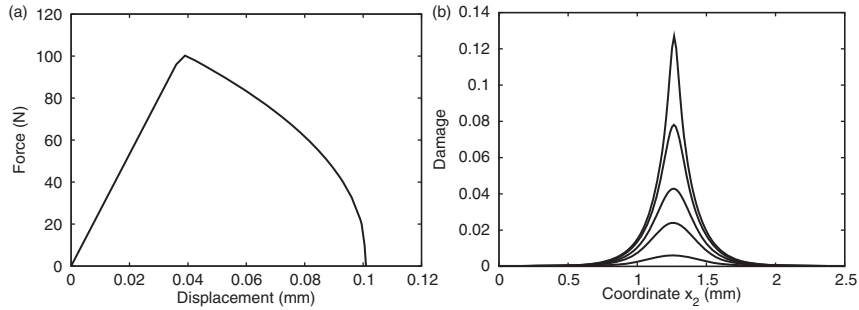

Figure 5. *Plots for a 1D softening rod with an exponentially decaying modulus. (a) Force vs. displacement diagram; (b) Shrinkage of the damage band.*

Crack Closure Effects

Finite element analysis of plasticity-induced fatigue crack growth necessitates particular investigation of crack closure phenomenon. The main mechanism behind crack closure is the large tensile plastic strains developed near the crack tip. In a cyclic loading regime, during unloading, previously initiated plastic strains are not fully recovered; therefore, behind the crack tip, formation of a plastic wake develops which reduces the driving force for crack growth. Moreover, during unloading, the zone near the crack tip which has already been plastically deformed, undergoes compression. The compressive residual stress in the vicinity of the crack tip strongly effects the crack tip driving force and a proper treatment in mechanical behavior becomes necessary.

In the literature, crack closure problem was first investigated by Elber (1970) and a more general overview for finite element analysis is recently presented by (Solanki et al., 2004). In this study, a special treatment of crack closure phenomenon has been established in the numerical model such that a previously damaged Gauss point deforms continuously, if the critical damage stress is reached under compressive forces ($\underline{\boldsymbol{n}}_d^s \cdot \tilde{\boldsymbol{\sigma}} \cdot \underline{\boldsymbol{n}}_d^s < 0$). In that condition, when the crack is unilaterally closed ($\delta_c^s \leq 0$) damage evolution stops ($\dot{\delta}_c^s = \dot{\delta}_i^s = 0$) as it is pointed out in the previous section.

Figure 6(a) demonstrates the crack closure behavior of a 1D specimen subjected to tensile and compressive forces respectively, where plasticity is excluded for a clear representation. The specimen is first broken under tension and then crack opening is closed under compression. Note that the specimen recovers its elastic behavior when the opening is entirely closed. Figure 6(b) shows the behavior of the same specimen under consecutive tensile and compressive forces without causing final fracture similar

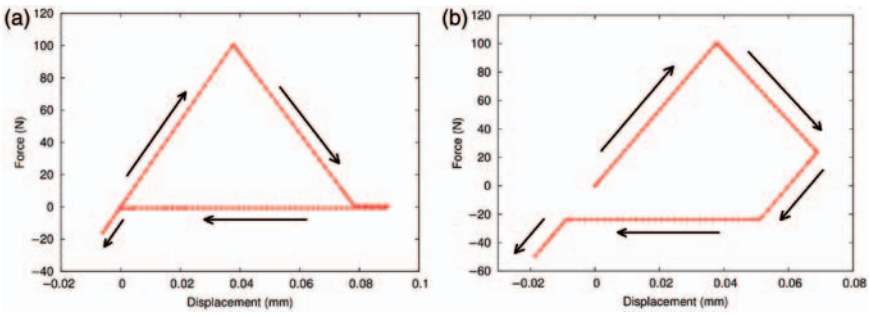

Figure 6. *Force vs. displacement diagram of a 1D softening rod under fatigue. (a) Final fracture occurs in the first cycle; (b) Material is damaged partially.*

to a possible loading cycle under fatigue. From the figure, one can also observe that during unloading and compression, elastic behavior is preserved up to the critical damage stress, Y_c, and the specimen deforms again continuously up to the crack closure. The value of critical damage stress does not change since the unrecoverable damage variable δ_{cum} stays constant due to the unilateral damage conditions. The corresponding finite element results are illustrated in Figure 7 (a) and an elastoplastic case for fatigue is shown up to final fracture in Figure 7 (b).

FINITE ELEMENT IMPLEMENTATION

Variational Formulation and Discretization

The variational formulation of the microdamage approach can be derived directly from the principle of virtual power (18):

$$-\int_{\Omega} p^{(i)} \mathrm{d}V + \int_{\partial\Omega} p^{(c)} \mathrm{d}S = 0 \tag{31}$$

$$-\int_{\Omega} (\underset{\sim}{\boldsymbol{\sigma}} : \dot{\underset{\sim}{\boldsymbol{\varepsilon}}} + a\, {}^{\chi}\dot{\delta} + \underline{\boldsymbol{b}}.\nabla\, {}^{\chi}\dot{\delta})\mathrm{d}V + \int_{\partial\Omega} (\underline{\boldsymbol{t}}.\dot{\underline{\boldsymbol{u}}} + a_c\, {}^{\chi}\dot{\delta})\mathrm{d}S = 0 \tag{32}$$

Finite element discretization of the displacement field $\underline{\boldsymbol{u}}$ and the microdamage field ${}^{\chi}\delta$ take the following form:

$$u = N_u d_u, \quad \nabla u = B_u d_u, \quad {}^{\chi}\delta = N_\delta d_\delta, \quad \nabla {}^{\chi}\delta = B_\delta d_\delta \tag{33}$$

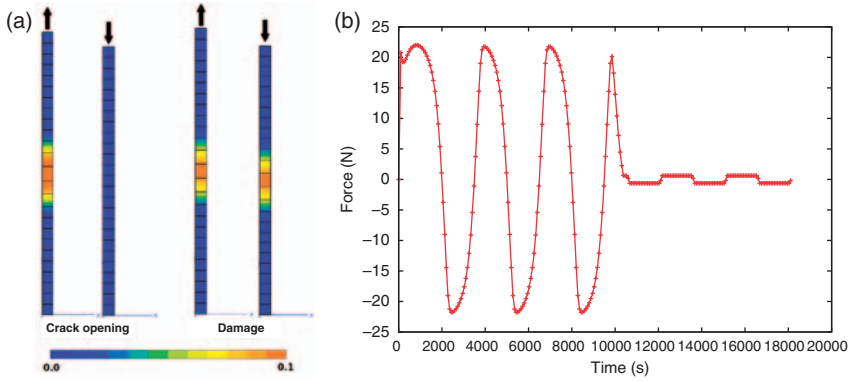

Figure 7. *(a) Demonstration of crack opening and damage evolution under cyclic loading for a 1D rod. (b) Representation of material damaging under fatigue.*

where d_u and d_δ are the nodal DOFs. N_u and N_δ represent the shape functions and B_u and B_δ stand for their partial derivatives with respect to the coordinates. In this study we use isoparametric quadratic elements for both types of DOFs ($N_u = N_\delta$).

Finally, the discretized equilibrium equations read:

$$\int_\Omega B_u^T \underset{\sim}{\sigma}\, \mathrm{d}V = \int_\Omega {N_u}^T \underline{\boldsymbol{f}} \mathrm{d}V + \int_\Gamma {N_u}^T \underline{\boldsymbol{t}}\, \mathrm{d}S \tag{34}$$

$$\int_\Omega ({N_\delta}^T a + {B_\delta}^T \underline{\boldsymbol{b}}) \mathrm{d}V = \int_\Gamma {N_\delta}^T a_c \mathrm{d}S \tag{35}$$

Implicit Incremental Formulation

A fully implicit Newton–Raphson incremental formulation is developed for solving (34) and (35). The corresponding time discretization is now introduced. Using the known values of the state variables $\underset{\sim}{\varepsilon}^e(t), \upsilon^s(t)$ (integrated from $\dot{\upsilon}^s = |\dot{\gamma}^s|$), $\delta^s_{c,i}(t)$, $\delta^s_{\mathrm{cum}}(t)$ for the current time step, the values at $t + \Delta t$ are estimated by a straight forward linearization procedure.

$$\underset{\sim}{\boldsymbol{\varepsilon}}^e(t+\Delta t) = \underbrace{\Delta t\ \dot{\underset{\sim}{\boldsymbol{\varepsilon}}}^e(t+\Delta t)}_{\Delta \underset{\sim}{\boldsymbol{\varepsilon}}^e} + \underset{\sim}{\boldsymbol{\varepsilon}}^e(t) \tag{36}$$

$$\upsilon^s(t+\Delta t) = \Delta t\ \dot{\upsilon}^s(t+\Delta t) + \upsilon^s(t) \tag{37}$$

$$\delta^s_{c,i}(t+\Delta t) = \Delta t\ \dot{\delta}^s_{c,i}(t+\Delta t) + \delta^s_{c,i}(t) \tag{38}$$

$$\delta^s_{\mathrm{cum}}(t+\Delta t) = \Delta t\ \dot{\delta}^s_{\mathrm{cum}}(t+\Delta t) + \delta^s_{\mathrm{cum}}(t) \tag{39}$$

Note that for the sake of simplicity, kinematic hardening variable is not included in this presentation. The necessary terms for the implementation are provided by (Cailletaud and Chaboche, 1995).

The presented model is implemented into the FE code ZeBuLoN (Besson et al., 1998), using a θ–method for the local integration. In order to calculate the state variable increments, the residuals and their Jacobian are written as follows:

$$R_{\underset{\sim}{\boldsymbol{\varepsilon}}^e} = \Delta \underset{\sim}{\boldsymbol{\varepsilon}}^e + \Delta \underset{\sim}{\boldsymbol{\varepsilon}}^p + \Delta \underset{\sim}{\boldsymbol{\varepsilon}}^d - \Delta \underset{\sim}{\boldsymbol{\varepsilon}} \tag{40}$$

$$= \Delta \varepsilon^e + \sum_{s=1}^{N_{\mathrm{slip}}} \underset{\sim}{\boldsymbol{m}}^s \Delta \upsilon^s \mathrm{sign}(\tau^s - x^s) \tag{41}$$

$$+\sum_{s=1}^{N_{\text{planes}}} \Delta\delta_c^s \underline{\boldsymbol{n}}_d^s \otimes \underline{\boldsymbol{n}}_d^s + \Delta\delta_i^s \underline{\boldsymbol{n}}_d^s \otimes \underline{\boldsymbol{l}}_{d_i}^s \ (i=1,2) \tag{42}$$

$$R_{\upsilon^s} = \Delta\upsilon^s - \Delta t \left\langle \frac{\Phi^s}{K} \right\rangle^n \tag{43}$$

$$R_{\delta_c^s} = \Delta\delta_c^s - \Delta t \left\langle \frac{f_c^s}{K_d} \right\rangle^{n_d} \text{sign}(\underline{\boldsymbol{n}}_d^s \cdot \underline{\underline{\boldsymbol{\sigma}}} \cdot \underline{\boldsymbol{n}}_d^s) \tag{44}$$

$$R_{\delta_i^s} = \Delta\delta_c^i - \Delta t \left\langle \frac{f_i^s}{K_d} \right\rangle^{n_d} \text{sign}(\underline{\boldsymbol{n}}_d^s \cdot \underline{\underline{\boldsymbol{\sigma}}} \cdot \underline{\boldsymbol{l}}_{d_i}^s) \tag{45}$$

$$R_{\delta_{\text{cum}}^s} = \Delta\delta_{\text{cum}} - \Delta\left(\sum_{s=1}^{N_{\text{planes}}} \left|\delta_c^s\right| + \left|\delta_1^s\right| + \left|\delta_2^s\right|\right) \tag{46}$$

$$[J] = \frac{\partial\{R\}}{\partial\{\Delta\vartheta\}} = 1 - \Delta t \frac{\partial\{\dot{\vartheta}\}}{\partial\{\Delta\vartheta\}}\bigg|_{t+\Delta t} \tag{47}$$

where $\{R\}^T = \{R_{\varepsilon^e},\ R_{\upsilon^s},\ R_{\delta_c^s},\ R_{\delta_i^s},\ R_{\delta_{\text{cum}}}\}$ and ϑ stands for the internal state variables to be integrated locally. Then, the Jacobian matrix becomes:

$$[J] = \begin{pmatrix} \frac{\partial R_{\varepsilon^e}}{\partial\Delta\varepsilon^e} & \frac{\partial R_{\varepsilon^e}}{\partial\Delta\upsilon^s} & \frac{\partial R_{\varepsilon^e}}{\partial\Delta\delta_c^s} & \frac{\partial R_{\varepsilon^e}}{\partial\Delta\delta_i^s} & \frac{\partial R_{\varepsilon^e}}{\partial\Delta\delta_{\text{cum}}} \\ \frac{\partial R_{\upsilon^s}}{\partial\Delta\varepsilon^e} & \frac{\partial R_{\upsilon^s}}{\partial\Delta\upsilon^e} & \frac{\partial R_{\upsilon^s}}{\partial\Delta\delta_c^s} & \frac{\partial R_{\upsilon^s}}{\partial\Delta\delta_i^s} & \frac{\partial R_{\upsilon^s}}{\partial\Delta\delta_{\text{cum}}} \\ \frac{\partial R_{\delta_c^s}}{\partial\Delta\varepsilon^e} & \frac{\partial R_{\delta_c^s}}{\partial\Delta\upsilon^e} & \frac{\partial R_{\delta_c^s}}{\partial\delta_c^s} & \frac{\partial R_{\delta_c^s}}{\partial\delta_{\text{cum}}} & \frac{\partial R_{\delta_c^s}}{\partial\delta_{\text{cum}}} \\ \frac{\partial R_{\delta_i^s}}{\partial\Delta\varepsilon^e} & \frac{\partial R_{\delta_i^s}}{\partial\Delta\upsilon^e} & \frac{\partial R_{\delta_i^s}}{\partial\delta_c^s} & \frac{\partial R_{\delta_i^s}}{\partial\delta_i^s} & \frac{\partial R_{\delta_i^s}}{\partial\delta_{\text{cum}}} \\ \frac{\partial R_{\delta_{\text{cum}}}}{\partial\Delta\varepsilon^e} & \frac{\partial R_{\delta_{\text{cum}}}}{\partial\Delta\upsilon^e} & \frac{\partial R_{\delta_{\text{cum}}}}{\partial\Delta\delta_i^s} & \frac{\partial R_{\delta_{\text{cum}}}}{\partial\Delta\delta_c^s} & \frac{\partial R_{\delta_{\text{cum}}}}{\partial\Delta\delta_{\text{cum}}} \end{pmatrix} \tag{48}$$

After convergence, the θ–method allows the calculation of the tangent matrix of the behavior. R can be decomposed into two parts as:

$$\{R\} = \{R_i\} - \{R_e\} \tag{49}$$

where R_e corresponds to the applied load. After the convergence (i.e. $\{R\} \approx \{0\}$), an infinitesimal variation can be applied to the residual equation such as:

$$\delta\{R\} = \{0\} = \delta\{R_i\} - \delta\{R_e\} \tag{50}$$

which can be rewritten in the form:

$$\delta\Delta\vartheta = [J]^{-1}\delta\{R_e\} \tag{51}$$

For the calculation of elastic strain increment, above relation reads:

$$\delta\Delta\underset{\sim}{\varepsilon}^e = \underset{\sim}{\boldsymbol{J}}_e\,\delta\Delta\underset{\sim}{\varepsilon}, \delta\Delta\underset{\sim}{\sigma} = \underset{\sim}{\boldsymbol{C}} : \underset{\sim}{\boldsymbol{J}}_e\,\delta\Delta\underset{\sim}{\varepsilon} \tag{52}$$

where $[\underset{\sim}{\boldsymbol{J}}_e]$ is the upper left part of $[J]^{-1}$:

$$[J]^{-1} = \begin{bmatrix} [\underset{\sim}{\boldsymbol{J}}_e] & [J_{ij}] \\ [J_{ji}] & [J_{jj}] \end{bmatrix} \tag{53}$$

Note that a consistent tangent matrix can directly be obtained from $[\underset{\sim}{\boldsymbol{C}} : \underset{\sim}{\boldsymbol{J}}_e]$ and it is non-symmetric, since the coupling between plasticity and damage is established in one way. The Jacobian matrix terms are provided in Tables 1–4.

MODEL VALIDATION

For the model validation, a 2D single crystal CT-like specimen under monotonic loading is analyzed. The corresponding finite element mesh is given in Figure 8. Analyses are performed for two different crack widths, obtained by furnishing different material parameters which control the size of intrinsic length scale, L (Figure 9). The propagation of a crack, corresponding stress fields and the comparison with classical elastic solutions are given in Figure 10. This comparison shows that the microdamage model is able to reproduce the elastic stress concentration at the crack tip except very

Table 1. Jacobian matrix terms for ε^e.

$\dfrac{\partial R_{\underset{\sim}{\varepsilon}^e}}{\partial\Delta\varepsilon^e} = \underset{\sim}{\boldsymbol{I}}$
$\dfrac{\partial R_{\underset{\sim}{\varepsilon}^e}}{\partial\Delta\upsilon^s} = \text{sign}(\tau^s - x^s)\underset{\sim}{\boldsymbol{m}}^s$
$\dfrac{\partial R_{\underset{\sim}{\varepsilon}^e}}{\partial\Delta\delta_c^s} = \underline{\boldsymbol{n}}_d^s \otimes \underline{\boldsymbol{n}}_d^s$
$\dfrac{\partial R_{\underset{\sim}{\varepsilon}^e}}{\partial\Delta\delta_i^s} = \underline{\boldsymbol{n}}_d^s \otimes \underline{\boldsymbol{l}}_{d_i}^s (n = 1, 2)$
$\dfrac{\partial R_{\underset{\sim}{\varepsilon}^e}}{\partial\Delta\delta_i^s} = 0$

Table 2. Jacobian matrix terms for υ^s.

$$\frac{\partial R_{\upsilon^s}}{\partial \Delta \underline{\underline{\varepsilon}}^e} = -\text{sign}(\tau^s - x^s)\, g(f)(\underline{\underline{\mathbf{c}}} : \underline{\underline{m}}^s), \qquad g(f) = \Delta t \left\langle \frac{\Phi^s}{K} \right\rangle^{n-1}$$

$$\frac{\partial R_{\upsilon^s}}{\partial \Delta \upsilon^e} = \underline{\underline{I}} - g(f)\frac{\partial \Phi^s}{\partial \upsilon^s}$$

$$\frac{\partial R_{\upsilon^s}}{\partial \Delta \delta^s_{c,i}} = 0$$

$$\frac{\partial R_{\upsilon^s}}{\partial \Delta \delta^s_{\text{cum}}} = 0$$

Table 3. Jacobian matrix terms for $\delta^s_{c,i}$.

$$\frac{\partial R_{\delta^s_c}}{\partial \Delta \underline{\underline{\varepsilon}}^e} = -h(f)\mathbf{c} : (\underline{\underline{n}}^s_d \otimes \underline{\underline{n}}^s_d), \qquad h(f) = \Delta t \frac{n_d}{K_d} \left\langle \frac{f^s_c}{K_d} \right\rangle^{n_d - 1}$$

$$\frac{\partial R_{\delta^s_i}}{\partial \Delta \underline{\underline{\varepsilon}}^e} = -h(f)\mathbf{c} : (\underline{\underline{n}}^s_d \otimes \underline{\underline{l}}^s_{d_i})$$

$$\frac{\partial R_{\delta^s_c}}{\partial \Delta \upsilon^s} = -\text{sign}(\underline{\underline{n}}^s_d \cdot \underline{\underline{\sigma}} \cdot \underline{\underline{n}}^s_d) h(f) \underline{\underline{\sigma}}\, n^c d e^{-d\gamma_{\text{cum}}}$$

$$\frac{\partial R_{\delta^s_i}}{\partial \Delta \upsilon^s} = -\text{sign}(\underline{\underline{n}}^s_d \cdot \underline{\underline{\sigma}} \cdot \underline{\underline{l}}^s_{d_i}) h(f) \sigma^c_n d e^{-d\gamma_{\text{cum}}}$$

$$\frac{\partial R_{\delta^s_{ci}}}{\partial \delta^s_{c,i}} = \underline{\underline{I}}$$

$$\frac{\partial R_{\delta^s_c}}{\partial \delta^s_{\text{cum}}} = \text{sign}(\underline{\underline{n}}^s_d \cdot \underline{\underline{\sigma}} \cdot \underline{\underline{n}}^s_d) h(f)^{\chi} H + \sum_{s=1}^{N_{\text{planes}}} \text{sign}(\underline{\underline{n}}^s_d \cdot \underline{\underline{\sigma}} \cdot \underline{\underline{n}}^s_d) h(f) H$$

$$\frac{\partial R_{\delta^s_i}}{\partial \delta^s_{\text{cum}}} = \text{sign}(\underline{\underline{n}}^s_d \cdot \underline{\underline{\sigma}} \cdot \underline{\underline{l}}^s_{d_i}) h(f)^{\chi} H + \sum_{s=1}^{N_{\text{planes}}} \text{sign}(\underline{\underline{n}}^s_{\text{d}} \cdot \underline{\underline{\sigma}} \cdot \underline{\underline{l}}^s_{\text{d}_i}) \text{h(f)H}$$

close to the crack tip where finite stress values are predicted. Moreover, the size of the zone of departure from the elastic solution is comparable with the size of the intrinsic length scale (process zone $\approx 3 \times L$).

Another 2D example, namely a plate under uniaxial tension with several cleavage planes, is investigated (Figure 11). In order to trigger localization,

Table 4. Jacobian matrix terms for δ_{cum}.

$\frac{\partial R_{\delta_{cum}}}{\partial \Delta \varepsilon^e} = 0$
$\frac{\partial R_{\delta_{cum}}}{\partial \Delta v^s} = 0$
$\frac{\partial R_{\delta_{cum}}}{\partial \Delta \delta_c^s} = -\text{sign}(\underline{n}_d^s \cdot \underline{\underline{\sigma}} \cdot \underline{n}_d^s)$
$\frac{\partial R_{\delta_{cum}}}{\partial \Delta \delta_i^s} = -\text{sign}(\underline{n}_d^s \cdot \underline{\underline{\sigma}} \cdot \underline{l}_{d_i}^s)$
$\frac{\partial R_{\delta_{cum}}}{\partial \Delta \delta_{cum}} = 1$

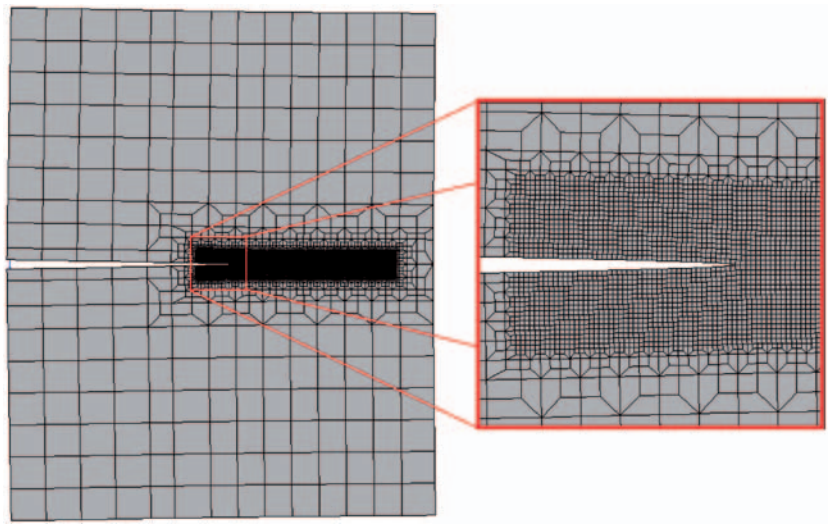

Figure 8. *Finite element mesh of the CT-like specimen.*

an initial geometric defect is created on the left edge. First, a cleavage plane is oriented at 30° from the horizontal axis. FEA results show that localization path is perfectly matching with the cleavage plane and the size of the localization band is controlled by ω in (29)(Figure 11 (a)). Second, two orthogonal cleavage planes are placed with an orientation of 45° from the horizontal axis representing {1 1 1} planes. For the former case,

damage–plasticity coupling leads to merged localization bands forming a straight crack path which can be considered as a type of ductile crack (Figure 11 (b)). For the latter case, plasticity is excluded from the calculation and crack path is allowed to choose its path between the orthogonal planes resulting in a brittle type of crack propagation (Figure 11 (c)). Corresponding FE results validate that the model is able to predict crack bifurcation. However, physical relevance of this fracture has to be investigated in the future.

APPLICATION TO FATIGUE CRACK GROWTH IN SINGLE CRYSTALS

In this section, the crack growth tests of superalloy PWA1483 performed at 950°C and presented in Marchal (2006) are simulated. For this purpose,

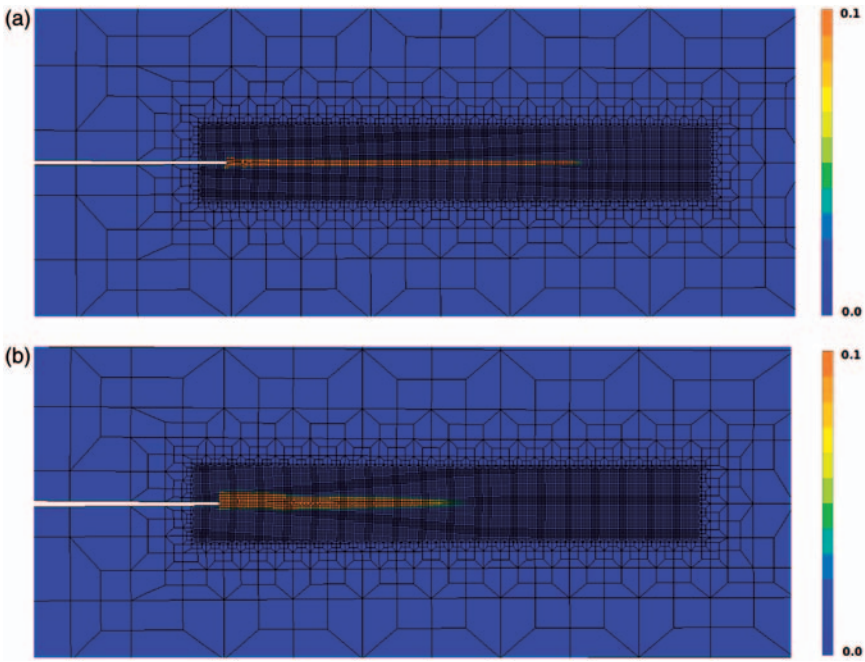

Figure 9. *Crack growth in a 2D single crystal CT-like specimen with a single cleavage plane aligned through the horizontal axis under vertical tension. Field variable* δ_{cum}*. (a)* $A=100\,\text{Mpa}\,\text{mm}^2$*,* $H=-20{,}000\,\text{Mpa}$ *and* ${}^{\chi}H=30{,}000\,\text{Mpa}$*; (b)* $A=150\,\text{MPa}\,\text{mm}^2$*,* $H=-10{,}000\,\text{MPa}$ *and* ${}^{\chi}H=30{,}000\,\text{MPa}$*.*

a standard SEN specimen geometry is used (Figure 12). The mesh and the boundary conditions are provided in Figure 13. As an initial defect, a 2.25 mm long artificial crack is introduced and the geometric symmetry is taken into account. Crack tip zone is regularly meshed and element size is

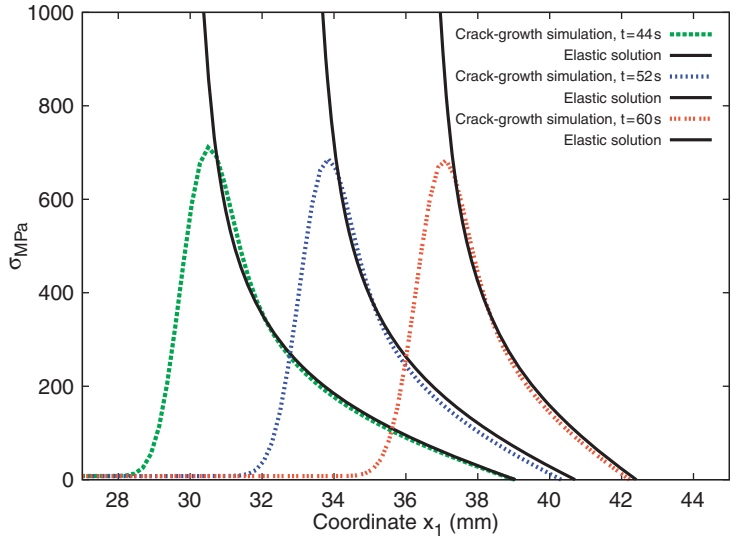

Figure 10. *Evolution of the crack and the stress fields in a CT-like specimen compared with corresponding elastic solutions.*

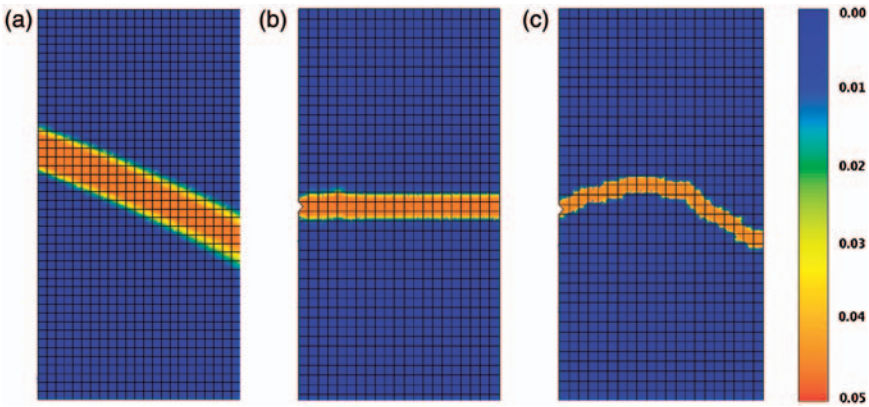

Figure 11. *Crack growth in a 2D single crystal block with a single inclined cleavage plane (a) and two orthogonal planes oriented at 45° (b), and (c) under vertical tension with 10 % strain. Field variable* δ_{cum}.

fixed to 2 μm which is considered as a representative value concerning crack growth in single crystals. All elements are chosen to be 2D quadratic 10-node bricks with reduced integration. A single cleavage plane is fixed to horizontal axis and the crack is oriented as (0 0 1)[1 0 0]. A sinusoidal cyclic loading regime is applied to the geometry with an R ratio = 0.1 with a frequency of 0.1 Hz as it is defined in Marchal (2006). The parameter identification procedure has been performed for $\Delta K = 25$, 35, 45 and 60 MPa$\sqrt{m}$ respectively, where ΔK is related to the applied force and the geometry with the relation:

$$K_I = \frac{F}{B\sqrt{w}} \left\{ \frac{\sqrt{2\tan(\frac{\pi a}{2w})}}{\cos(\frac{\pi a}{2w})} \left[0.752 + 2.02\frac{a}{w} + 0.37\left[1 - \sin(\frac{\pi a}{2w})\right]^3 \right] \right\} \tag{54}$$

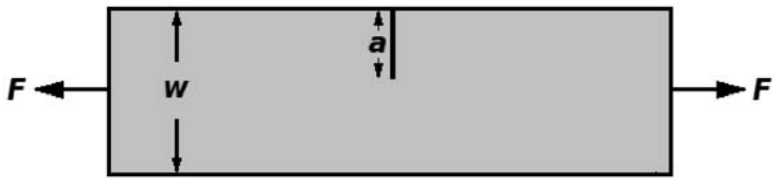

Figure 12. *Illustration of a SEN geometry corresponding to the Equation (54), where B is the specimen thickness.*

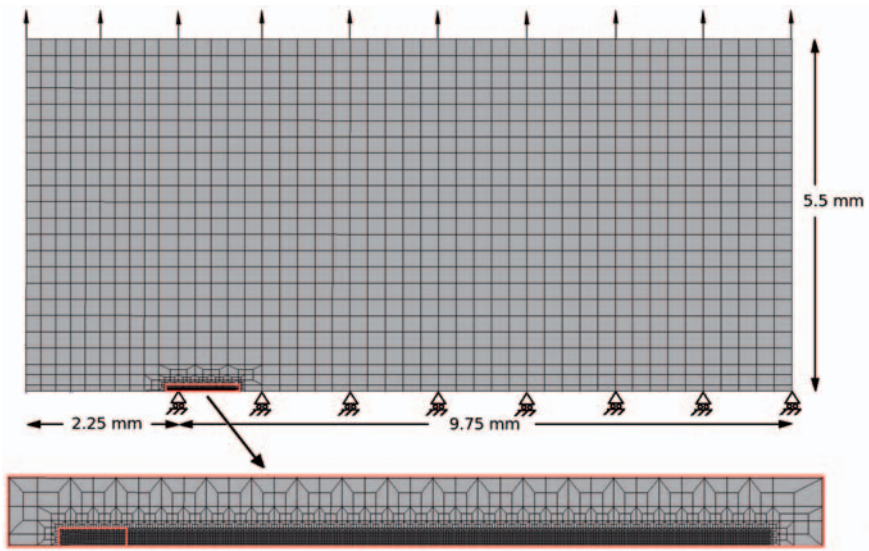

Figure 13. *Illustration of the finite element mesh of the SEN specimen with boundary conditions.*

The parameter values used for the life-time prediction are provided in Table 5. One can observe that parameters for the Norton rule are taken in the same order of plastic parameters. A and ${}^{\chi}H$ which mainly control the characteristic length were identified in order to obtain a damage band size of 8 μm for the full geometry. The parameters Θ, σ_n^c and H control the crack

Table 5. Microdamage parameters for the life-time assessment of PWA1483.

Parameters	A (MPa mm^2)	Θ	Kd (MPa s$^{1/n}$)	nd	σ_n^c (MPa)	${}^{\chi}H$ (MPa)	H (MPa)	σ_{ult} (MPa)
Values	2.0	3.0	550	6.5	1200	30000	−15000	0.1

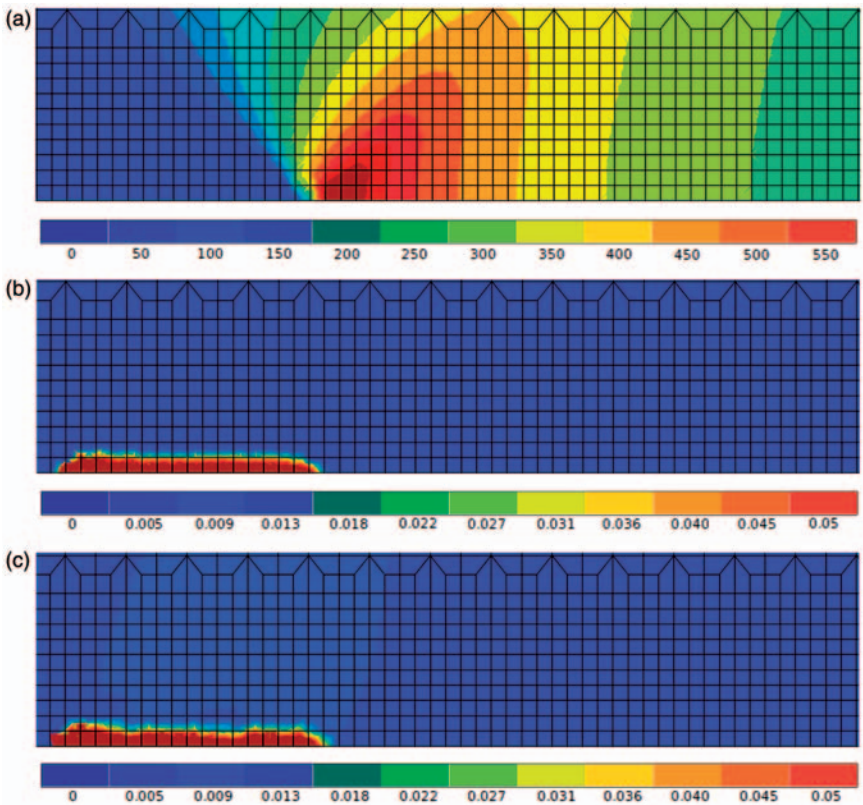

Figure 14. *Demonstration of the FEA results of the SEN specimen after 10 cycles for (a) opening stress, σ_{22}, (b) cumulative damage, δ_{cum} and (c) plastic strain normal to the crack propagation direction, ε_{22}^p.*

initiation and crack growth rate. Therefore, they were identified from the experimental data provided in Figure 15. The initial threshold value for ΔK determines the σ_n^c and from the slope of the da/dN versus ΔK diagram, one can identify the parameters Θ, H. Several FEA results are shown in Figure 14. First, FEA maps for opening stress, σ_{22} are provided. As it is noticed from the figure, the stress field perfectly moves with the crack tip and the broken elements undergo zero stress representing a realistic crack. The exact place of the crack tip can be easily tracked by the damage field demonstrated at the middle and the plastic wake zone induced by the crack growth is presented underneath. The ability of the model to predict crack growth rate is demonstrated in Figure 15. Experimental and numerical results indicate that model predictions are in good agreement with the experimental observations. The parameter values used for the life-time prediction are provided in Table 5.

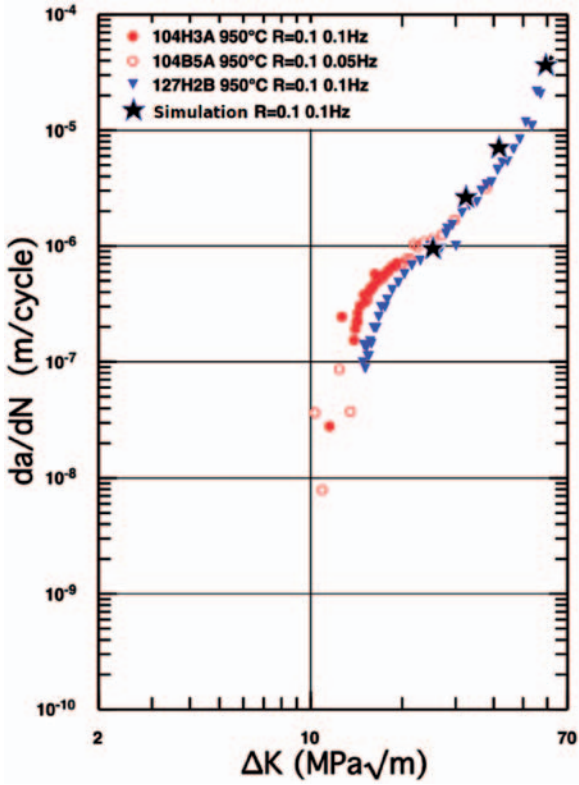

Figure 15. *Comparison between the numerical simulation and the experimental data of the fatigue test performed for PWA1483.*

CONCLUSION

A numerical model of fatigue crack growth in single crystals based on microdamage theory is proposed. First, the crystal plasticity model coupled to continuum damage is presented. The damage initiation is strongly related with the accumulated plastic slip, through the damage threshold function. Then, the approach is further developed by conducting a regularization procedure based on microdamage continuum. A 1D geometry is scrutinized for the observation of stable critical damage stress evolution and the crack closure phenomenon. It has been shown that the model is capable of simulating crack closure in the desired way successfully.

After giving the details of numerical implementation procedure, the model is validated through several 2D specimens under monotonic loading. The results have shown that the model is able to reproduce the elastic stress concentration at the crack tip and predict the crack bifurcation by defining multi-plane damage systems which could be considered as the main advantage compared to the CZMs where the crack paths are predefined. After the model validation, a parameter fitting procedure is performed in order to simulate the crack growth tests performed on single crystal PWA1483 at 950°C. A standard SEN specimen has been analyzed for several ΔK values and a good agreement between the experimental data and the numerical results has been found.

As a prospective issue, introducing a multi-plane damage system, a bifurcation analysis under realistic creep-fatigue loadings are to be considered. The influence of crystal orientation and mixed mode loadings (modes I and II) on crack growth rate are to be investigated. Moreover, combining crystal plasticity, continuum damage and a strain gradient formulation, the model possess a great potential for modeling fatigue crack growth in polycrystals.

ACKNOWLEDGMENT

The authors gratefully acknowledged the support of the European Commission within project PREMECCY with the contract number AST5-CT-2006-030889.

REFERENCES

Aslan, O. and Forest, S. (2009). Crack Growth Modelling in Single Crystals Based on Higher Order Continua, *Computational Materials Science*, **45**: 756–761.

Aswath, P. (1994). The Effect of Orientation on Crystallographic Cracking in Notched Nickel-base Supperalloy Single Crystal Subjected to Far-field Cyclic Compression, *Metallurgical and Materials Transactions*, **25A**: 287–297.

Besson, J. (2009). Damage of Ductile Materials Deforming Under Multiple Plastic or Viscoplastic Mechanisms, *International Journal of Plasticity*, **25**: 2204–2221.

Besson, J., Leriche, R., Foerch, R. and Cailletaud, G. (1998). Object–oriented Programming Applied to the Finite Element Method. Part ii, *Application to material behaviours*. *Revue Européenne des Eléments Finis*, **7**: 567–588.

Bouvard, J.L., Chaboche, J.L., Feyel, F. and Gallerneau, F. (2009). A Cohesive Zone Model for Fatigue and Creep-fatigue Crack Growth in Single Crystal Superalloys, *International Journal of Fatigue*, **31**: 868–879.

Cailletaud, G. and Chaboche, J.L. (1995). Integration Methods for Complex Plastic Constitutive Equations, *Computer Methods in Applied Mechanics and Engineering*, **133**: 125–155.

Crompton, J.S. and Martin, J.W. (1984). Crack Tip Plasticity and Crack Growth in a Single-crystal Superalloy at Elevated Temperatures, *Materials Science and Engineering*, **64**: 37–43.

Dillard, T., Forest, S. and Ienny, P. (2006). Micromorphic Continuum Modelling of the Deformation and Fracture Behaviour of Nickel Foams, *European Journal of Mechanics A/Solids*, **25**: 526–549.

Ekh, M., Lillbacka, R. and Runesson, K. (2004). A Model Framework for Anisotropic Damage Coupled to Crystal (Visco) Plasticity, *International Journal of Plasticity*, **20**: 2143–2159.

Elber, W. (1970). Fatigue Crack Closure Under Cyclic Tension, *Engineering Fracture Mechanics*, **2**: 37–45.

Engelen, R.A.B., Geers, M.G.D. and Baaijens, F.P.T. (2003). Nonlocal Implicit Gradient-enhanced Elasto-plasticity for the Modelling of Softening Behaviour, *International Journal of Plasticity*, **19**: 403–433.

Eringen, A.C. and Suhubi, E.S. (1964). Nonlinear Theory of Simple Microelastic Solids, *International Journal of Engineering Science*, **2**: 189–203, 389-404.

Forest, S. (2009). The Micromorphic Approach for Gradient Elasticity, Viscoplasticity and Damage, *ASCE Journal of Engineering Mechanics*, **135**: 117–131.

Gall, K., Sehitoglu, H. and Kadioglu, Y. (1996). FEM Study of Fatigue Crack Closure Under Double Slip, *Acta Metallurgica*, **44**: 3955–3965.

Germain, N., Besson, J. and Feyel, F. (2007). Simulation of Laminate Composites Degradation Using Mesoscopic Non–local Damage Model and Non–local Layered Shell Element, *Modelling and Simulation in Materials Science and Engineering*, **15**: S425–S434.

Gurson, A.L. (1977). Continuum Theory of Ductile Rupture by Void Nucleation and Growth. part i: Yield Criteria and Flow Rules for Porous Ductile Media, *Journal of Engineering Materials and Technology*, **99**: 2–15.

Kiyak, Y., Fedelich, B. and Pfennig, A. (2007). Simulation of Crack Growth Under Low Cycle Fatigue at High Temperature in a Single Crystal Superalloy, *Engineering Fracture Mechanics*, **75**: 2418–2443.

Lemaitre, J. and Chaboche, J.-L. (1994). *Mechanics of Solid Materials*, Cambridge, UK, University Press.

Leverant, G. and Gell, M. (1975). The Influence of Temperature and Cyclic Frequency on the Fatigue Fracture of Cube Oriented Nickel-based Supperalloy, *Metallurgical Transactions A*, **6A**: 367–371.

Marchal, N. (2006). Propagation de Fissure en Fatigue-fluage á Haute Température de Superalliages Monocristallins à Base de Nickel, PhD Thesis, Ecole des Mines de Paris.

Mahnken, R. (2002). Theoretical, Numerical and Identification Aspects of a New Model Class for Ductile Damage, *International Journal of Plasticity*, **18**: 801–831.

Marchal, N., Flouriot, S., Forest, S. and Remy, L. (2006b). Crack–tip Stress–Strain Fields in Single Crystal Nickel–base Superalloys at High Temperature Under Cyclic Loading, *Computational Materials Science*, **37**: 42–50.

Marchal, N., Forest, S., Rémy, L. and Duvinage, S. (2006a). Simulation of Fatigue Crack Growth in Single Crystal Superalloys Using Local Approach to Fracture. In: Moinereau, D., Steglich, D. and Besson, J. (eds), *Local Approach to Fracture, 9th European Mechanics of Materials Conference, Euromech–Mecamat,* Moret–sur–Loing, France, Presses de l'Ecole des Mines de Paris, pp. 353–358.

Murakami, S., Hayakawa, K. and Liu, Y. (1998). Damage Evolution and Damage Surface of Elastic-plastic-damage Materials Under Multiaxial Loading, *International Journal of Damage Mechanics*, **7**: 103–128.

Musienko, A. and Cailletaud, G. (2009). Simulation of Inter- and Transgranular Crack Propagation in Polycrystalline Aggregates due to Stress Corrosion Cracking, *Acta Materialia*, **57**: 3840–3855.

Nouailhas, D. and Cailletaud, G. (1995). Tension-torsion Behavior of Singlecrystal Supperalloys: Experiment and Finite Element Analysis, *International Journal of Plasticity*, **11**: 451–470.

Parisot, R., Forest, S., Pineau, A., Nguyen, F., Démonet, X. and Mataigne, J.-M. (2004). Deformation and Damage Mechanisms of Zinc Coatings on Hot-dip Galvanized Steel Sheets: Part ii. Damage Modes, *Metallurgical and Materials Transactions A*, **35A**: 813–823.

Peerlings, R.H.J., Geers, M.G.D., de Borst, R. and Brekelmans, W.A.M. (2001). A Critical Comparison of Nonlocal and Gradient–enhanced Softening Continua, *International Journal of Solids Structures*, **38**: 7723–7746.

Peerlings, R.H.J., Massart, T.J. and Geers, M.G.D. (2004). A Thermodynamically Motivated Implicit Gradient Damage Framework and its Application to Brick Masonry Cracking, *Computer Methods in Applied Mechanics and Engineering*, **193**: 3403–3417.

Qi, W. and Bertram, A. (1999). Anisotropic Continuum Damage Modeling for Single Crystals at High Temperatures, *International Journal of Plasticity*, **15**: 1197–1215.

Rice, J.R. (1987). Tensile Crack Tip Fields in Elastic-ideally Plastic Crystals, *Mechanics of Materials*, **6**: 317–335.

Simo, J.C. and Ju, J.W. (1989). Finite Deformation Damage-elastoplasticity: A Non-conventional Framework, *International Journal of Computational Mechanics*, **5**: 375–400.

Solanki K., Daniewicz S.R. and Newman Jr, J.C. (2004). Finite Element Analysis of Plasticity-induced Fatigue Crack Closure, *Engineering Fracture Mechanics*, **71**: 149–171.

Tvergaard, V. and Needleman, A. (1984). Analysis of Cup-cone Fracture in a Round Tensile Bar, *Acta Metallurgica*, **32**: 157–169.

Voyiadjis, G.Z. and Deliktas, B. (2000). A Coupled Anisotropic Damage Model for the Inelastic Response of Composite Materials, *Computer Methods in Applied Mechanics and Engineering*, **183**: 159–199.